



Discovery and Characterization of a Potent and Selective Inhibitor of *Aedes aegypti* Inward Rectifier Potassium Channels

Rene Raphemot^{1,2}, Matthew F. Rouhier³, Daniel R. Swale¹, Emily Days⁴, C. David Weaver^{2,4}, Kimberly M. Lovell^{2,6}, Leah C. Konkel^{2,6}, Darren W. Engers^{2,6}, Sean F. Bollinger^{2,6}, Corey Hopkins^{2,5,6}, Peter M. Piermarini^{3*}, Jerod S. Denton^{1,2,4,5*}

1 Department of Anesthesiology, Vanderbilt University Medical Center, Nashville, TN, United States of America, **2** Department of Pharmacology, Vanderbilt University School of Medicine, Nashville, TN, United States of America, **3** Department of Entomology, Ohio Agricultural Research and Development Center, The Ohio State University, Wooster, OH, United States of America, **4** Institute of Chemical Biology, Vanderbilt University School of Medicine, Nashville, TN, United States of America, **5** Institute for Global Health, Vanderbilt University, Nashville, TN, United States of America, **6** Department of Chemistry, Vanderbilt University School of Medicine, Nashville TN, United States of America

Abstract

Vector-borne diseases such as dengue fever and malaria, which are transmitted by infected female mosquitoes, affect nearly half of the world's population. The emergence of insecticide-resistant mosquito populations is reducing the effectiveness of conventional insecticides and threatening current vector control strategies, which has created an urgent need to identify new molecular targets against which novel classes of insecticides can be developed. We previously demonstrated that small molecule inhibitors of mammalian Kir channels represent promising chemicals for new mosquitocide development. In this study, high-throughput screening of approximately 30,000 chemically diverse small-molecules was employed to discover potent and selective inhibitors of *Aedes aegypti* Kir1 (AeKir1) channels heterologously expressed in HEK293 cells. Of 283 confirmed screening 'hits', the small-molecule inhibitor VU625 was selected for lead optimization and in vivo studies based on its potency and selectivity toward AeKir1, and tractability for medicinal chemistry. In patch clamp electrophysiology experiments of HEK293 cells, VU625 inhibits AeKir1 with an IC₅₀ value of 96.8 nM, making VU625 the most potent inhibitor of AeKir1 described to date. Furthermore, electrophysiology experiments in *Xenopus* oocytes revealed that VU625 is a weak inhibitor of AeKir2B. Surprisingly, injection of VU625 failed to elicit significant effects on mosquito behavior, urine excretion, or survival. However, when co-injected with probenecid, VU625 inhibited the excretory capacity of mosquitoes and was toxic, suggesting that the compound is a substrate of organic anion and/or ATP-binding cassette (ABC) transporters. The dose-toxicity relationship of VU625 (when co-injected with probenecid) is biphasic, which is consistent with the molecule inhibiting both AeKir1 and AeKir2B with different potencies. This study demonstrates proof-of-concept that potent and highly selective inhibitors of mosquito Kir channels can be developed using conventional drug discovery approaches. Furthermore, it reinforces the notion that the physical and chemical properties that determine a compound's bioavailability in vivo will be critical in determining the efficacy of Kir channel inhibitors as insecticides.

Citation: Raphemot R, Rouhier MF, Swale DR, Days E, Weaver CD, et al. (2014) Discovery and Characterization of a Potent and Selective Inhibitor of *Aedes aegypti* Inward Rectifier Potassium Channels. PLoS ONE 9(11): e110772. doi:10.1371/journal.pone.0110772

Editor: Joseph Clifton Dickens, United States Department of Agriculture, Beltsville Agricultural Research Center, United States of America

Received: June 9, 2014; **Accepted:** September 16, 2014; **Published:** November 6, 2014

Copyright: © 2014 Raphemot et al. This is an open-access article distributed under the terms of the Creative Commons Attribution License, which permits unrestricted use, distribution, and reproduction in any medium, provided the original author and source are credited.

Data Availability: The authors confirm that all data underlying the findings are fully available without restriction. All relevant data are contained within the paper.

Funding: This work was funded by a grant from the Foundation for the National Institutes of Health through the Vector-Based Transmission of Control: Discovery Research (VCTR) program of the Grand Challenges in Global Health initiative. This work was also supported in part by a grant from the National Institute of Diabetes and Digestive and Kidney Diseases (1R01DK082884; JSD). The funders had no role in study design, data collection and analysis, decision to publish, or preparation of the manuscript.

Competing Interests: The authors have declared that no competing interests exist.

* Email: piermarini.1@osu.edu (PMP); jerod.s.denton@vanderbilt.edu (JSD)

Introduction

Mosquitoes are vectors of protozoan, filarial nematode, and viral pathogens that cause numerous human diseases, including malaria, lymphatic filariasis, and dengue fever. These diseases impose an enormous burden on global health and profoundly impair socioeconomic advancement in developing countries [1]. The overuse of a limited number of insecticides has led to the emergence of insecticide-resistant populations of mosquitoes, which is hampering the effectiveness of vector control efforts

[2,3,4]. Consequently, there is a need to identify new molecular targets against which insecticides can be developed and deployed.

An emerging body of evidence from our group supports the idea that inward rectifier potassium (Kir) channels represent viable targets for insecticide development [5,6,7]. Kir channels are tetrameric proteins that conduct K⁺ ions across the cell membrane and thereby generate an ionic current that underlies various cellular functions. Dipteran insects possess three major Kir channel subtypes, denoted Kir1, Kir2 and Kir3. In *Drosophila melanogaster*, there are three genes that encode Kir channels

(*DrKir1*, *DrKir2*, *DrKir3*), which play important roles in osmoregulation, immunity, and development [8,9,10,11]. In *Aedes aegypti*, there are five Kir channel genes (*AeKir1*, *AeKir2A*, *AeKir2B*, *AeKir2B'* and *AeKir3*), which are expressed in various body segments and tissues such as the carcass (thorax and abdomen), head, Malpighian tubules, midgut, and hindgut [6,12]. We showed previously in vitro that the *A. aegypti* Kir1 (*AeKir1*) channel mediates strong inward rectifying K⁺ currents that are blocked by barium and the small molecule inhibitors, VU573 and VU590 [7,12,13]. Moreover, a hemolymph injection of either VU573 or VU590 inhibits the excretion of urine by adult female mosquitoes, leads to abdominal bloating, and incapacitates mosquitoes within 24 h [5].

Taken together, the above studies indicate that Kir channels represent promising molecular targets for insecticides that have a novel mechanism of action by disrupting the renal-dependent regulation of extracellular fluid homeostasis (i.e., renal failure). However, in mammals, Kir channels regulate the electrical excitability of neurons and cardiac cells, hormone secretion, and transport of K⁺ ions across epithelial tissues of the kidney and gut [14]. Missense mutations that perturb the activity of Kir channels cause human diseases of the heart, nervous system, pancreas, and kidney [15,16,17]. Thus, efforts aimed at developing insecticides to target Kir channels must verify that lead compounds do not perturb the functions of mammalian Kir channels.

As such, the above 'tool' compounds VU573 and VU590 allowed us to establish proof-of-concept, but are not suitable for insecticide development, in part, because they inhibit mammalian Kir channels with greater potency than *AeKir1* [18,19]. Here, we aim to discover new chemical probes of *AeKir1* channels that exhibit improved potency and selectivity compared to the tool compounds by optimizing and validating an existing fluorescent thallium (Tl⁺) flux-based assay of *AeKir1* function [5] for high-throughput screening (HTS) of small molecule libraries. Screening approximately 30,000 small molecules from the chemical library of the Vanderbilt Institute of Chemical Biology (VICB) resulted in the identification of 283 compounds with activity against *AeKir1* channels. We focus on the in vitro and in vivo activity of one of these compounds, N-(3-methoxyphenyl)-2-methyl-1-propionylindoline-5-sulfonamide (VU625), which exhibits nanomolar affinity and is highly selective for *AeKir1* over mammalian Kir channels.

Materials and Methods

Tl⁺ flux assays

Tl⁺ flux assays were performed essentially as described previously [13,18,19]. Briefly, stably transfected T-Rex-HEK-293 cells expressing *AeKir1* channels were cultured overnight in 384-well plates (20,000 cells/20 μ L/well black-walled, clear-bottomed BD PureCoat amine-coated plates (BD, Bedford, MA) with a plating media containing DMEM, 10% dialyzed FBS and 1 μ g/mL tetracycline. The next day, the cell culture medium was replaced with a dye-loading solution containing assay buffer (Hanks Balanced Salt Solution with 20 mM HEPES, pH 7.3), 0.01% (*w/v*) Pluronic F-127 (Life Technologies, Carlsbad, CA), and 1.2 μ M of the thallium-sensitive dye Thallos-AM (TEFlabs, Austin, TX). Following 1 hr incubation at room temperature, the dye-loading solution was washed from the plates and replaced with 20 μ L/well of assay buffer.

The plates were transferred to a Hamamatsu Functional Drug Screening System 6000 (FDSS6000; Hamamatsu, Hamamatsu (or Bridgewater, NJ), Japan) where 20 μ L/well of test compounds in assay buffer (as prepared below) were added and allowed to incubate with the cells for 20 min. After the incubation period, a

baseline recording was collected at 1 Hz for 10 s (excitation 470 \pm 20 nm, emission 540 \pm 30 nm) followed by a Tl⁺ stimulus buffer addition (10 μ L/well) and data collection for an additional 4 min. The Tl⁺ stimulus buffer contains in (mM) 125 NaHCO₃, 1.8 CaSO₄, 1 MgSO₄, 5 glucose, 12 Tl₂SO₄, 10 HEPES, pH 7.4. For Tl⁺ flux assays on the mammalian channels Kir2.x, Kir4.1 and Kir6.2/SUR1 expressing cells, the Tl⁺ stimulus buffer contained 1.8 mM Tl₂SO₄. Also, Tl⁺ flux assays on Kir3.1/3.2/mGlu8 expressing cell, required addition of an EC₈₀ concentration of glutamate (Sigma-Aldrich, St. Louis, MO) with the Tl⁺ stimulus buffer [19].

The test compounds were transferred to daughter polypropylene 384-well plates (Greiner Bio-One, Monroe, NC) using an Echo555 liquid handler (Labcyte, Sunnyvale, CA), and then diluted into assay buffer to generate a 2X stock in 0.6% DMSO (0.3% final). For Tl⁺ flux assays on Kir6.2/SUR1 expressing cells, test compounds were diluted in assay buffer containing diazoxide (250 μ M final) to induce channel activation [20]. Concentration-response curves (CRCs) were generated by screening compounds at 3-fold dilution series in 4-point (1 μ M–30 μ M) or 11-point (1 nM–30 μ M) CRCs.

Tl⁺ flux data were analyzed as previously described [19,21,22] using a combination of Excel (Microsoft Corp, Redmond, WA) with XLfit add-in (IDBS, Guildford, Surrey, UK) and OriginPro (OriginLab, Northampton, MA) software. Raw data were opened in Excel and each data point in a given trace was divided by the first data point from that trace (static ratio) followed by subtraction of data points from control traces generated in the presence of vehicle controls. The slope of the fluorescence increase beginning 5 s after Tl⁺ addition and ending 15 s after Tl⁺ addition was calculated.

Compound synthesis

2,2,2-trifluoro-1-(2-methylindolin-1-yl)ethan-1-one. The reagents and conditions are illustrated in Figure S1. To a round bottom flask equipped with a magnetic stir bar, 2-methylindoline (4.8 mL, 37 mmol, 1 eq.) and pyridine (46 mL) were added. The reaction mixture was cooled to 0°C and trifluoroacetic anhydride (6.3 mL, 44 mmol, 1.2 eq.) was added dropwise. The reaction mixture was allowed to warm to room temperature and was stirred an additional 2 hours. The reaction was quenched with water (50 mL) and diluted with DCM (100 mL). The organic layer was separated and washed subsequently with water (50 mL) and brine (50 mL), dried over Na₂SO₄, and concentrated under reduced pressure. The crude material (8.33g, 98%) was used without purification. LCMS: R_T = 0.785 min, [M+H]⁺ = 229.6; >98%.

2-methyl-1-(2,2,2-trifluoroacetyl)indoline-5-sulfonyl chloride: Chlorosulfonic acid (22 mL, 330 mmol, 9 equiv.) was added to a 100 mL round bottom flask equipped with a reflux condenser, and cooled to 0°C. To this, 2,2,2-trifluoro-1-(2-methylindolin-1-yl)ethan-1-one, (8.5 g, 37 mmol, 1 eq.) was added dropwise. The reaction mixture was removed from the ice bath. The vial was heated to 40°C for 1 hour. The reaction was subsequently cooled to room temperature and PCl₅ (7.7 g, 37 mmol, 1 equiv.) was added slowly. After gas evolution ceased, the reaction mixture was heated to 80°C for 1 hour. The reaction mixture was cooled to room temperature and then placed in an ice bath. Water was added very slowly to the reaction mixture. Subsequently, DCM was added and the reaction was filtered through a phase separator. The organic layer was concentrated under reduced pressure and used without subsequent purification (6.46 g, 53%).

N-(3-methoxyphenyl)-2-methylindoline-5-sulfonamide: 2-methyl-1-(2,2,2-trifluoroacetyl)indoline-5-sulfonyl chloride (2.5 g,

7.6 mmol, 1 eq.) was diluted with DCM (10 mL). 3-methoxyaniline (1.71 mL, 15.2 mmol, 2 eq.) followed by *N,N*-Diisopropylethylamine (5.3 mL, 31 mmol, 4 eq.) was added to the reaction. Reaction progress was monitored by LCMS. Once the reaction was deemed complete, it was diluted with DCM (40 mL) and washed with water (2x, 50 mL) and brine (50 mL). The organic layer was dried over Na_2SO_4 and concentrated under reduced pressure. Purification by flash chromatography (0%–100% EtOAc in Hexanes) afforded the desired product (2.66 g, 85%). LCMS: $R_T = 0.800$ min., $[\text{M} + \text{H}]^+ = 414.7$; >98% @ 220 and @ 254 nm. The trifluoroacetate was removed by stirring in a 1:1:1 mixture of MeOH, THF, and 10% NaOH affording the title compound (782 mg, 38%). LCMS: $R_T = 0.665$ min., $[\text{M} + \text{H}]^+ = 318.8$; >98% @ 220 and @ 254 nm.

N-(3-methoxyphenyl)-2-methyl-1-propionylindoline-5-sulfonamide (VU0077625): N-(3-methoxyphenyl)-2-methylindoline-5-sulfonamide (11 mg, 0.035 mmol, 1 eq.) was diluted with DCM (0.3 mL). To this reaction, pyridine was added (0.011 mL, 0.14 mmol, 4 eq.) followed by propionyl chloride (0.003 mL, 0.05 mmol, 1.5 eq.). Reaction progress was monitored by LCMS. Once the reaction was deemed complete it was concentrated under forced air and heat and was subsequently purified on preparative HPLC (3 mg, 26%). ^1H NMR (400.1 MHz, CDCl_3) δ ppm: 8.17 (bs, 1 H); 7.67 (dd, $J = 1.69, 8.72$ Hz, 1 H); 7.58 (s, 1 H); 7.16 (t, $J = 8.25$ Hz, 1 H); 6.69–6.57 (m, 4 H); 4.58 (bs, 1 H); 3.74 (s, 3 H); 3.38–3.32 (m, 1 H); 2.66–2.47 (m, 4 H); 1.29–1.22 (m, 5 H). HRMS (TOF, ES^+) $\text{C}_{19}\text{H}_{23}\text{N}_2\text{O}_4\text{S}$ $[\text{M} + \text{H}]^+$ calc'd for 375.1379, found 375.1381.

Patch clamp electrophysiology

T-REx-HEK293-*AeKir1* cells were voltage clamped in the whole-cell configuration of the patch clamp technique after overnight induction with tetracycline (1 $\mu\text{g}/\text{ml}$) essentially as described earlier [5]. Briefly, patch electrodes were pulled from silanized 1.5 mm outer diameter borosilicate microhematocrit tubes using a Narishige PC-10 two-stage puller. Electrode resistance ranged from 3.5 to 5.5 $\text{M}\Omega$ when filled with the following intracellular solution (in mM): 135 KCl, 2 MgCl_2 , 1 EGTA, 10 HEPES free acid, 2 Na_2ATP (Roche, Indianapolis, IN), pH 7.3, 275 mOsm. The standard bath solution contained (in mM): 135 NaCl, 5 KCl, 2 CaCl_2 , 1 MgCl_2 , 5 glucose, 10 HEPES free acid, pH 7.4, 290 mOsm. Whole-cell currents were recorded under voltage-clamp conditions using an Axopatch 200B amplifier (Molecular Devices, Sunnyvale, CA). Electrical connections to the amplifier were made using Ag/AgCl wires and 3 M KCl/agar bridges. Electrophysiological data were collected at 5 kHz and filtered at 1 kHz. Data acquisition and analysis were performed using pClamp 9.2 software (Axon Instruments). All recordings were made at room temperature (20–23°C).

Heterologous expression of *AeKir1* and *AeKir2B* in *Xenopus* oocytes

AeKir1 and *AeKir2B* channels were expressed heterologously in *Xenopus laevis* oocytes as described previously [6]. In brief, defolliculated *Xenopus* oocytes (purchased from Ecocyte Bioscience, Austin, TX) were injected with 10 ng (0.35 ng/nL) of either *AeKir1* or *AeKir2B* cRNA and cultured for 3–7 days in OR3 media at 18°C. Oocytes injected with 28 nl of nuclease-free H_2O served as controls.

Electrophysiology of *Xenopus* oocytes

All electrophysiological experiments on *Xenopus* oocytes were performed at room temperature. The compositions of the solutions used in these experiments are shown in Table 1. When present,

VU625 was dissolved in solution III or solution V to a final concentration of 0.1, 1, 5, 15, or 50 μM (0.05% DMSO). All solutions were delivered by gravity to a RC-3Z oocyte chamber (Warner Instruments, Hamden, CT) via polyethylene tubing at a flow rate of ~ 2 ml/min. Solution changes were made with a Rheodyne Teflon 8-way Rotary valve (Model 5012, Rheodyne, Rohnert Park, CA).

Electrophysiological recordings from oocytes were conducted as described previously [6]. In brief, each oocyte was transferred to the holding chamber under superfusion with solution I and impaled with two conventional-glass microelectrodes backfilled with 3 M KCl (resistances of 0.5–1.5 $\text{M}\Omega$) to measure membrane potential (V_m) and whole-cell membrane current (I_m), respectively. Current-voltage (I–V) relationships of oocytes were acquired as described previously [6]. In brief, the oocytes were subjected to a voltage-stepping protocol consisting of 20 mV steps from -140 mV to $+40$ mV (100 ms each). After the conclusion of the voltage-stepping protocol, the clamp was turned off and a new solution was superfused through the chamber for ~ 90 s before acquiring another I–V relationship. All V_m and I_m values were recorded by a Digidata 1440A Data Acquisition System (Molecular Devices) and the Clampex module of pCLAMP. The I–V plots were generated using the Clampfit module of pCLAMP.

To evaluate the inhibition of *AeKir1* and *AeKir2B* activity by VU625, we focused on the maximal inward currents elicited by the voltage-stepping protocol, which occur at a voltage of -140 mV. For *AeKir1* oocytes, the background, inward currents in solution II (i.e., 0.5 mM K^+) were subtracted from those in 1) solution III (i.e., 10 mM K^+) to calculate the total inward current for an oocyte before exposure to VU625 (I_A), and 2) solution III with VU625 to calculate the inward current after exposure to the small molecule (I_B). The percent inhibition of the inward current was calculated by subtracting I_B from I_A and then dividing by I_A . For *AeKir2B* oocytes, a similar protocol was followed and similar calculations were made, except solution IV replaced solution II and solution V replaced solution III.

Mosquito colony

The *Aedes aegypti* mosquito colony used in the present study is identical to that described previously [6]. As before, only adult female mosquitoes 3–10 days post emergence were utilized for experiments.

Mosquito toxicology experiments

Adult female mosquitoes for injection were anesthetized on ice and impaled through the metapleuron using a pulled-glass capillary attached to a nanoliter injector (Nanoject II, Drummond Scientific Company, Broomall, PA). Each mosquito received a single hemolymph injection of 69 nL of solution. The injection solution consisted of a potassium-rich phosphate buffered saline (K^+ -PBS), 15% DMSO, 1% β -cyclodextrin, 0.1% Solutol, and a concentration of VU625 to deliver the doses indicated. In experiments where probenecid was used, water-soluble probenecid (Biotium, Hayward CA) was included in the injection solution at 50 mM, thereby providing a dose of 3.4 nmol per mosquito.

The K^+ -PBS solution consisted of the following in mM: 92.2 NaCl, 47.5 KCl, 10 Na_2HPO_4 , and 2 KH_2PO_4 (pH 7.5). A total of 10 mosquitoes were injected for a given treatment or dose, and then were placed into small cages within a rearing chamber (28°C, 80% relative humidity, 12:12 light:dark) and allowed free access to a solution of 10% sucrose. The mosquitoes were observed at 24 hr after injection. For each treatment, 3–7 replicates of 10 mosquitoes each were performed.

Table 1. Compositions (in mM) of solutions used in *Xenopus* oocyte electrophysiology.

Solution #	I	II	III	IV	V
NaCl	96	88.5	88.5	73.5	73.5
NMDG-Cl	0	9.5	0	24.5	0
KCl	2	0.5	10	0.5	25
MgCl ₂	1.0	1.0	1.0	1.0	1.0
CaCl ₂	1.8	1.8	1.8	1.8	1.8
HEPES	5	5	5	5	5

The pH of all solutions was adjusted to 7.5 with NMDG-OH.

The osmolality of each solution was verified to be 190 mOsm kg⁻¹ H₂O (±5 mOsm kg⁻¹ H₂O) by vapor pressure osmometry.

NMDG = N-methyl-D-glucamine.

doi:10.1371/journal.pone.0110772.t001

Mosquito excretion experiments

The excretory capacity of mosquitoes was measured as described [6]. In brief, after anesthetizing mosquitoes on ice, their hemolymph was injected as described above with 900 nL of a K⁺-PBS vehicle containing 1.15% DMSO, 0.077% β-cyclodextrin, and 0.008% Solutol, or the vehicle containing VU625 (0.77 mM) to deliver a dose of 690 pmol of VU625 per mosquito. In experiments where probenecid was used, the vehicle was supplemented with water-soluble probenecid (3.08 mM) to deliver a dose of 3.4 nmol of probenecid per mosquito. After injection, the mosquitoes were placed immediately in a graduated, packed-cell volume tube (MidSci, St. Louis, MO; 5 mosquitoes per tube) and held at 28°C. The volume of urine excreted at 60 min post injection was measured as described previously [6], and all mosquitoes were confirmed to be alive at the end of 60 min period. For each treatment, 6–18 independent trials of 5 mosquitoes per treatment were performed.

Statistical analyses

TI⁺ flux assay. The Z' value was calculated as described earlier [21], using the following formula:

$$Z' = 1 - (3SD_p + 3SD_n) / |Mean_p + Mean_n|$$

where SD is standard deviation, p and n are vehicle control and compound inhibited flux values respectively.

To compare the effect of DMSO on *AeKir1*-mediated TI⁺ flux, a one-way ANOVA was performed with a Tukey's multiple comparison test. Prism software (GraphPad Software) was used to generate CRC from TI⁺ flux. Half-inhibition concentration (IC₅₀) values were calculated from fits using a four parameter logistic equation.

Mosquito toxicology and urine excretion. Prism (GraphPad Software) was used to generate a dose-response curve for the toxicity of VU625; the doses (x-axis) were first log transformed and then the mortality data was normalized using Prism, where the smallest value and largest values in a data set equal '0%' and '100%', respectively. The data were then fitted using a 'biphasic' algorithm (<100 constraint) to calculate potencies (ED₂₅ and ED₇₅ values). To compare 1) the toxic effects among the vehicle, probenecid, VU625, and VU625 + probenecid treatments, and 2) the excretory capacity among the vehicle, probenecid, VU625, and VU625 + probenecid treatments, one-way ANOVAs were performed with Newman-Keuls posttests.

Results

Discovery of novel *AeKir1* inhibitors via HTS

In an effort to discover mosquito-specific inhibitors of *AeKir1*, we optimized a TI⁺ flux assay for HTS of large libraries of chemically diverse small molecules. The assay utilizes a monoclonal T-REx-HEK293 cell line that expresses *AeKir1* from a tetracycline-inducible promoter [5]. The fluorescent dye, Thallos, is used to report the inward flux of TI⁺ through the *AeKir1* channel pore in a population of cells plated in individual wells of a 384-well plate. As shown in Figure 1A, overnight induction of *AeKir1* expression with tetracycline leads to a robust TI⁺ flux compared to control cells that were not treated with tetracycline. This assay enables more than 300 compounds to be tested simultaneously in a single plate, and thousands of compounds to be tested daily, for effects on *AeKir1* activity.

The assay was validated for HTS by meeting a series of performance benchmarks. First, the assay was tested for its tolerance to the small-molecule vehicle DMSO at concentrations up to 10% v/v. As shown in Fig. 1B, the TI⁺-flux mediated by *AeKir1* is unaffected by DMSO concentrations up to 1.3% v/v as compared to the 0% DMSO control (one-way ANOVA, P < 0.0001). Next, the assay was tested for uniformity and reproducibility of HTS performance. As shown in Fig. 1C, the average Z' statistic for these experiments was 0.69±0.05 (Z'≥0.5 is suitable for HTS), indicating that the assay is robust and will enable modulators of *AeKir1* to be identified in HTS with a low false-positive rate.

Approximately 30,000 compounds from the VICB library were screened at a nominal concentration of 10 μM for inhibition of *AeKir1*. From this primary screen and following confirmation testing in tetracycline-induced and uninduced T-REx-HEK293-*AeKir1* cells (see Methods), 283 authentic channel-dependent modulators were selected for further study. Because our ultimate goal is to develop Kir channel inhibitors that are active against mosquitoes and not humans, these 'hits' were subsequently tested for dose-dependent activity against a panel of mammalian Kir channels, which included Kir1.1, Kir2.1, Kir2.2, Kir2.3, Kir3.1/3.2, Kir4.1, Kir7.1(M125R), and Kir6.2/SUR1 [18,19,21]. Four-point concentration response curves (CRCs) were generated for the 283 compounds, resulting in 17 inhibitors with 11 unique chemical scaffolds that exhibited dose-dependent inhibition of *AeKir1* with IC₅₀ values below 5 μM and little to no activity (IC₅₀≥30 μM) against mammalian Kir channels (data not shown). These compounds were subsequently purchased from commercial vendors, freshly dissolved in DMSO, and assayed in 11-point CRCs against *AeKir1* via the TI⁺-flux assay.

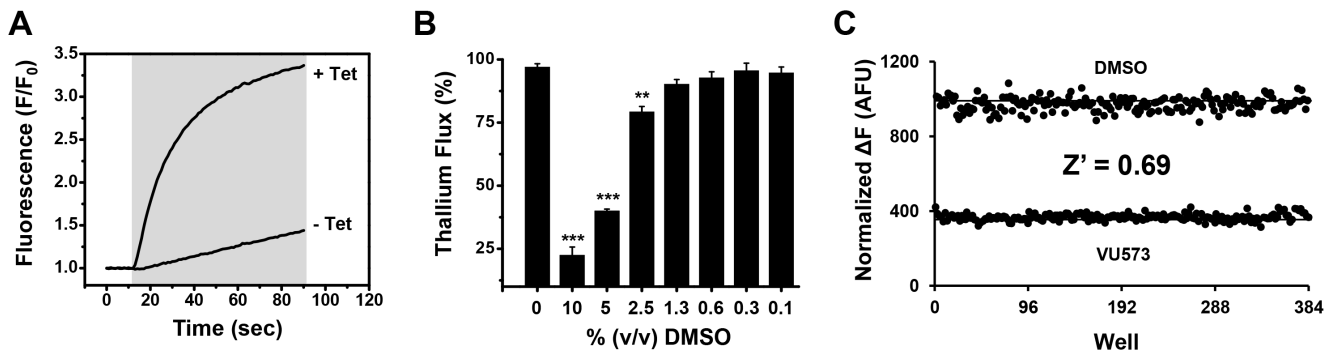


Figure 1. Ti^+ flux assay of *AeKir1* channel activity for high-throughput screening. (A) Representative Ti^+ -induced changes in Thallo fluorescence in T-Rex-HEK293-*AeKir1* cells cultured overnight with (+Tet) or without (-Tet) tetracycline. The shaded box indicates the cell exposure to Ti^+ . (B) DMSO concentrations up to 1.3% v/v DMSO have no effect on Ti^+ flux through *AeKir1*. Data are means \pm SEM ($n = 3$). One-way ANOVA $P < 0.0001$, and asterisks (**, ***) indicate $P < 0.01$ or $P < 0.001$ respectively, when compared to 0% DMSO (Tukey's test). (C) Representative checkerboard analysis using 100 μM VU573 or 0.1% v/v DMSO as the vehicle control. The mean peak fluorescence amplitude of each sample population is indicated with a solid line and alternating samples for DMSO (top) and VU573 (bottom) are graphed as individual points. The mean \pm SD Z' calculated over 6 plates on 3 separate days was 0.69 ± 0.05 . doi:10.1371/journal.pone.0110772.g001

VU625 is a potent and preferential inhibitor of *AeKir1* vs. mammalian Kir and *AeKir2B* channels

From the aforementioned Ti^+ flux assays, one compound—N-(3-methoxyphenyl)-2-methyl-1-propionylindoline-5-sulfonamide, termed VU625—was found to inhibit *AeKir1* in 11-point CRCs with an IC_{50} of 0.32 μM (95% CI: 0.25–0.39 μM) and a Hill coefficient value of 0.98 (95% CI: 0.8–1.2) (Fig. 2A–C). VU625 also had no significant effects on the mammalian Kir channels assayed via Ti^+ flux with the exception of G-protein coupled Kir channels comprised of Kir3.1/3.2 subunits ($\text{IC}_{50} = 8.6 \mu\text{M}$; Table S1). Furthermore, in radioligand displacement assays against 68 mammalian GPCR's, ion channels, and transporters, 10 μM VU625 was active (defined as $>50\%$ ligand displacement) against only three targets: adenosine A1 receptor (76% displacement), melatonin MT1 receptor (56% displacement) and 5-HT_{2B} receptor (69% displacement) (Table S2).

To further confirm the activity of VU625 obtained from Ti^+ -flux assays, we used patch-clamp electrophysiology to assay the inhibition of *AeKir1* expressed in T-REx-HEK293 cells. In whole-cell patch clamp recordings, VU625 inhibited *AeKir1* channel

activity with an IC_{50} of 96.8 nM (95% CI: 75.4–124.2 nM) and a Hill coefficient value of 1.02 (95% CI: 0.8–1.3) (Fig. 3A, B).

In a previous paper, we demonstrated that other small molecule inhibitors of *AeKir1* (i.e., VU573 and VU590) can have different pharmacological effects on *AeKir2B* [6]. Thus, we sought to determine the effects of VU625 on *AeKir2B* channel activity, utilizing *Xenopus* oocytes heterologously expressing *AeKir2B*. *AeKir1* expressing oocytes served as positive controls. Figure 3C shows that VU625 inhibits *AeKir1*- and *AeKir2B*-mediated K^+ currents with IC_{50} values of 3.8 μM (95% CI: 2.3–6.3 μM) and 45.1 μM (95% CI: 31.7–64.2 μM), respectively. Thus, VU625 inhibits both *AeKir1* and *AeKir2B* channels, albeit with greater affinity for *AeKir1*. It should be noted that the reduction in VU625 potency observed in *Xenopus* oocytes compared to HEK cells is typical for a small-molecule inhibitor of Kir channels and has been observed for structurally diverse compounds and Kir channels [5,6,19,23].

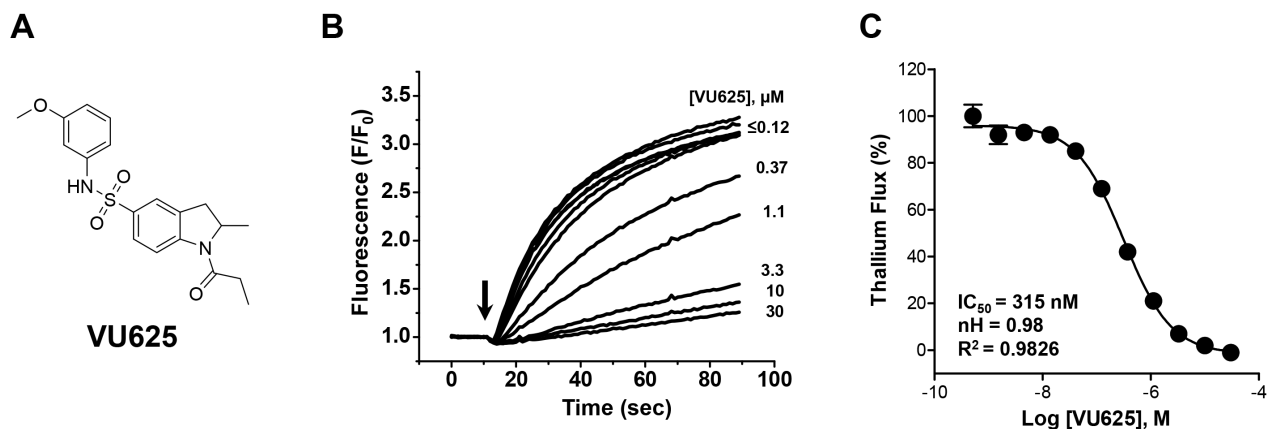


Figure 2. VU625 is a potent inhibitor of *AeKir1* in Ti^+ flux assays. (A) Chemical structure of VU625. (B) Dose-dependent inhibition of the *AeKir1*-mediated Ti^+ flux by VU625 with concentrations ranging from ≤ 0.12 to 30 μM . The arrow indicates when Ti^+ was added to the extracellular bath. (C) Concentration-response curves of VU625 derived from Ti^+ flux assays. The IC_{50} and Hill-coefficient ($n\text{H}$) values are 315 nM (95% CI: 254.4–390.2 nM) and 0.98 respectively. Data are mean \pm SEM. $n = 4$ independent experiments performed in triplicate. doi:10.1371/journal.pone.0110772.g002

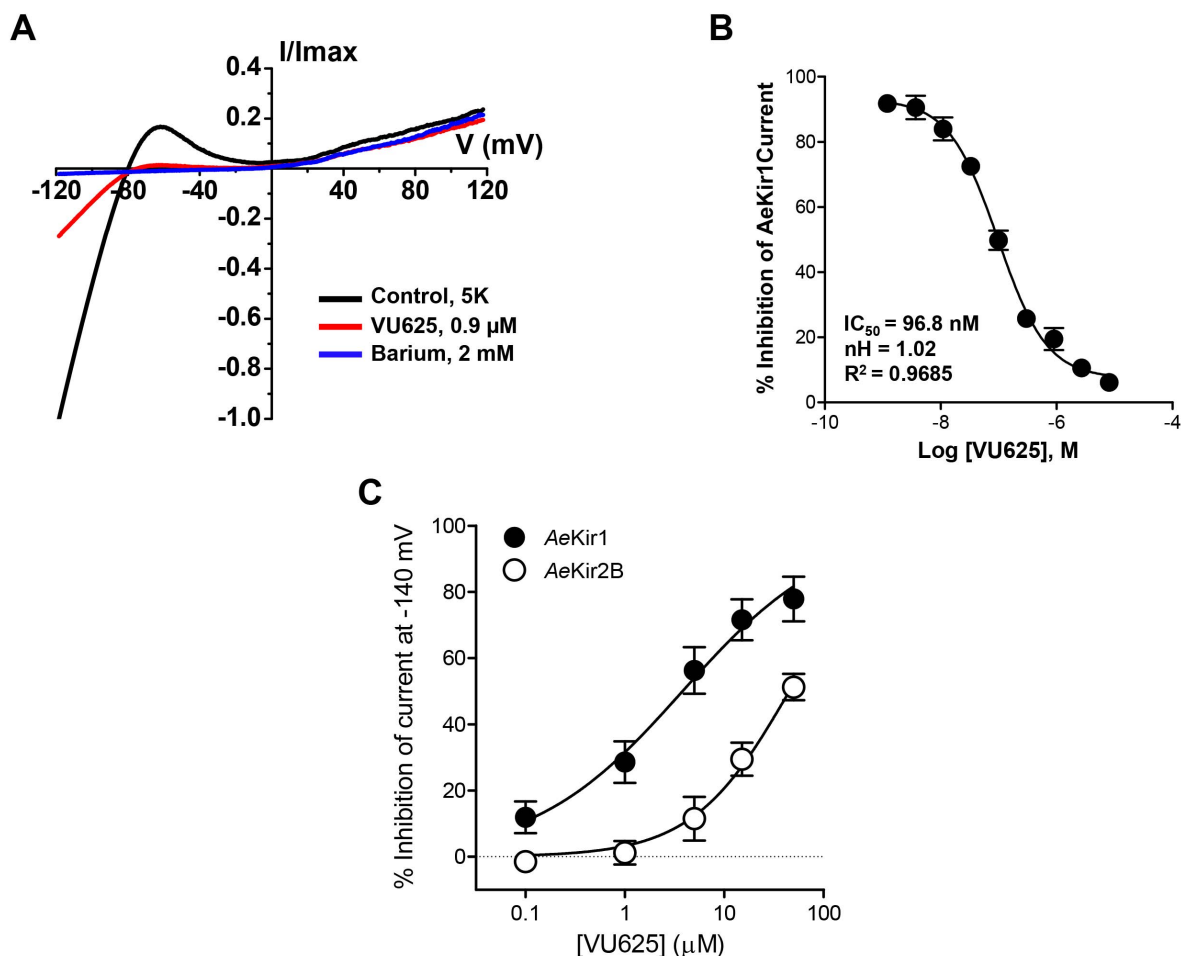


Figure 3. VU625 is a potent and preferential inhibitor of AeKir1 over AeKir2B in whole-cell electrophysiology. (A) Normalized AeKir1 current-voltage relationships obtained from heterologous expression in T-Rex-HEK293 cells, illustrating VU625-dependent inhibition before (control) and after addition of 0.9 μM VU625. Residual AeKir1 currents were inhibited with 2 mM barium. Cells were voltage clamped at -75 mV and ramped between -120 mV and +60 mV. (B) Concentration-response curve of VU625 derived from patch clamp experiments ($n=4-6$). The IC₅₀ of VU625 is 96.8 nM (95% CI: 75.4–124.2 nM). (C) Concentration-response curves of current inhibition mediated by heterologous expression in *Xenopus* oocytes of AeKir1 (filled circles) and AeKir2B (open circles) channels after bath application of VU625. $n=4-5$ oocytes per concentration. The calculated IC₅₀ values of VU625 for AeKir1 and AeKir2B current inhibition are 3.8 μM (95% CI: 2.3–6.3 μM) and 45.1 μM (95% CI: 31.7–64.2 μM), respectively. doi:10.1371/journal.pone.0110772.g003

Chemical lead optimization and structure-activity relationships

Because of its potency, clean ancillary pharmacology and chemical tractability (Figures 2–3, Tables S1–S2), VU625 was selected for lead optimization (**3a**, Table 2). We partitioned the compound into three areas for structure-activity relationship (SAR) exploration denoted as the sulfonamide, central core, and southern amide portions (Fig. 4A). The first generation libraries held the sulfonamide and the central core sections constant and diversified the southern amide portion (Table 2). The synthetic scheme (Fig. 4B) for this portion was straightforward and started with protection of the amine with trifluoroacetamide (TFAA, pyridine) followed by sulfonyl chloride formation (ClSO₂, PCl₅). Next, the sulfonamide was formed, the protecting group was removed, and either the amide or sulfonamide was formed (see Methods for details). Little tolerance for steric bulk was seen in this portion of the molecule. That is, the trifluoroacetamide (VU0477197, **3b**, Table 2) retained potency (0.58 μM), however, larger aromatic amides were much less active (**3c–g**, Table 2). The same trend was observed for the sulfonamide compounds, with

smaller sulfonamides retaining nanomolar activity (VU0477691, **3k**, 0.76 μM; VU0477692, **3l**, 0.82 μM) and the larger aromatic group leading to less activity (**3h**, Table 2).

Next, we evaluated the left-hand sulfonamide portion of the molecule, however, all efforts to change the 3-methoxyaryl moiety led to significant reductions in potency (see Table S3). Finally, we explored the central core with the intent of establishing the minimal pharmacophore needed for activity against AeKir1. To this end, the indoline core was replaced with simple aryl, heteroaryl or biaryl groups which all led to compounds with much reduced activity (>10-fold loss of potency). However, an interesting SAR was seen with very closely related 6,6- or 6,5-indole or dihydroquinolinone-like structures (**4a–f**, Table 3). The simple *N*-methyl indole (VU0481807, **4a**, 0.55 μM, Table 3) retained most of the activity as VU625 and addition of a 2-methyl (VU0486620, **4b**, 0.97 μM, Table 3) led to a further minor reduction in activity. Expanding the ring system and addition of a lactam (**4c–e**, Table 3) was not productive. Lastly, removal of the methyl group in the indoline system of VU625, led to a ~3-fold loss of potency (VU0483404, **4f**, 1.15 μM, Table 3).

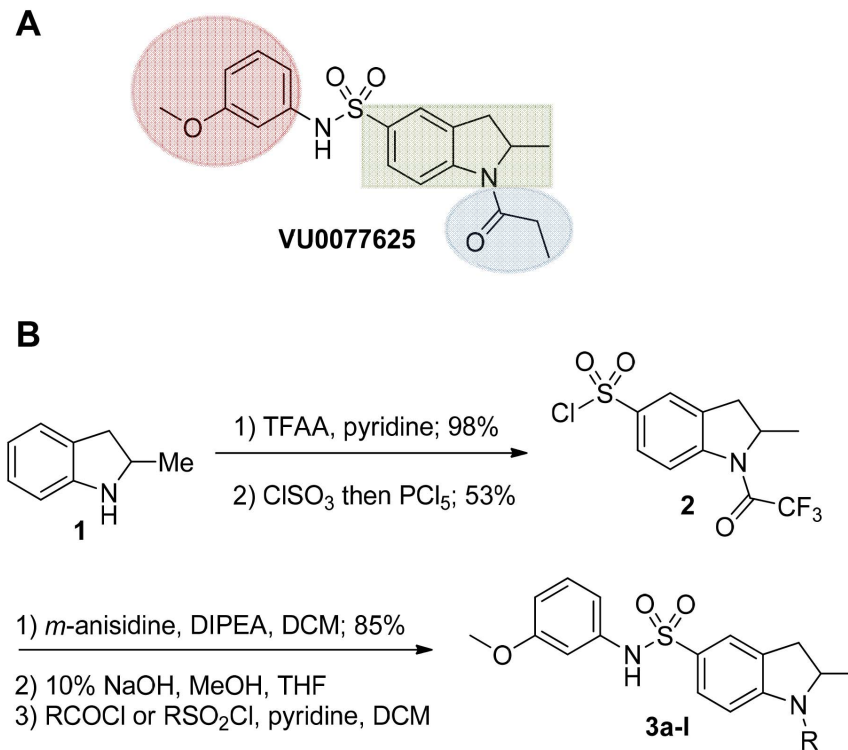


Figure 4. Design and chemical lead optimization strategy for VU625. (A) Modular approach to assess three areas of diversification of VU625: sulfonamide (red shading), central core (green shading), and southern amide (blue shading) portions. (B) General synthetic approach to access VU625 and analogs around the amide and sulfonamide portions.
doi:10.1371/journal.pone.0110772.g004

Figure 5 summarizes the SAR observed for the VU625 scaffold. The left-hand sulfonamide portion offered the least amount of SAR traction as only the 3-methoxyphenyl (and weaker 2-methoxyphenyl) sulfonamide provided activity. Replacement with an amide, or substituting the 3-methoxyphenyl for other aryl groups all led to less potent compounds. Replacement of the propanamide in the southern fraction was tolerated as long as the substituent was small and aliphatic. Sulfonamides could be exchanged, although there was an observed ~2-3-fold loss of activity. Lastly, the central core was also important for potency. Only very similar compounds such as indole and des-methyl indoline were tolerated.

VU625-induced toxicity is increased by probenecid

Injection of the *AeKir1* channel inhibitors VU573 or VU590 into the hemolymph of adult female *A. aegypti* mosquitoes leads to their incapacitation and/or death within 24 h [5,6]. Surprisingly, injection of a high dose (i.e. 690 pmol per mosquito) of VU625, which is a more potent inhibitor of *AeKir1* than VU573 and VU590, into the hemolymph of mosquitoes had no significant effects on mosquito behavior or survival within 24 h (Fig. 6). Thus, we hypothesized that the lack of *in vivo* effects could be due to poor bioavailability of VU625 as a result of metabolic detoxification and/or excretion by the mosquito.

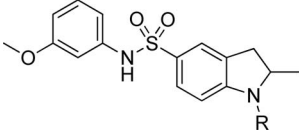
We therefore tested whether probenecid, which is a broad-spectrum inhibitor of organic anion transporters (OATs) and ATP-binding cassette (ABC) transporters [24,25,26], would improve the efficacy of VU625. Interestingly, both probenecid and VU625 have a sulfonamide moiety in their chemical structure (Fig. S2). As shown in Fig. 6, the injection of probenecid (3.4 nmol per mosquito) along with VU625 (690 pmol per mosquito)

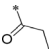
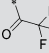
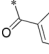
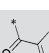
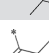

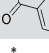
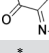
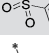
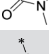
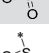
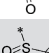
significantly increases the toxicity of VU625 within 24 h compared to injection of VU625 or probenecid alone. The abdomens of these mosquitoes were not severely bloated and obvious sub-lethal effects (e.g., loss of flight) were not apparent.

We next sought to characterize the dose-response relationship of VU625 in mosquitoes when co-injected with a constant dose of probenecid (3.4 nmol per mosquito). As shown in Fig. 7, co-injection of VU625 with probenecid induces mortality in mosquitoes within 24 h in a biphasic manner with 25% and 75% efficacious doses (ED₂₅ and ED₇₅) of 9.96 pmol and 502 pmol, respectively. This biphasic dose-response relationship suggests the inhibition of at least two distinct molecular targets for which VU625 has different affinities, which is consistent with the inhibition of both *AeKir1* and *AeKir2B* channels by VU625 (Fig. 3C).

VU625-induced reduction of urine excretion is enhanced by probenecid

We showed previously that pharmacological inhibition of *AeKir1* with the small molecule inhibitors VU573 and VU590 leads to a decrease in the excretory capacity of *A. aegypti* mosquitoes after loading their hemolymph with 900 nl of a PBS vehicle [5] [6]. Therefore, we sought to similarly determine the effects of VU625 on mosquito excretory capacity. As shown in Fig. 8, mosquitoes injected with the PBS vehicle excreted 644±24.18 nL of urine within the next hour. Consistent with the toxicity studies, we found that adding VU625 (0.77 mM) to the vehicle, which delivers 690 pmol of VU625 per mosquito, did not significantly decrease the excretory capacity (583.3±29.52 nL/female) compared to the vehicle controls (Fig. 8). Interestingly, adding probenecid (50 mM) to the vehicle, which delivers

Table 2. Structure-activity relationships and lead optimization summary of VU0077625 scaffold.


Cmpd	R	VU#	IC ₅₀ ±SEM (μM)
3a		VU0077625	0.36±0.02
3b		VU0477197	0.58±0.04
3c		VU0477684	5.20±0.40
3d		VU0477693	4.41±1.11
3e		VU0477694	3.87±1.97
3f		VU0477688	>30
3g		VU0477685	4.40±0.50
3h		VU0477686	3.29±0.89
3i		VU0477687	2.09±0.49
3j		VU0477690	2.82±0.48
3k		VU0477691	0.76±0.00
3l		VU0477692	0.82±0.48

IC₅₀ values were derived from 11-point CRCs on *AeKir1* in Tl⁺ flux experiments performed in triplicate on two separate days.
doi:10.1371/journal.pone.0110772.t002

3.4 nmol of probenecid per mosquito, causes a small but significant reduction in excretory capacity to 467.8±33.53 nL/female, suggesting a potential role of probenecid-sensitive transporters in urine excretion. However, adding both VU625 (0.77 mM) and probenecid (50 mM) to the vehicle significantly decreases the excretory capacity the furthest to 236.7±24.53 nL/female.

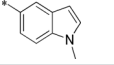
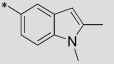
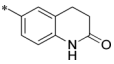
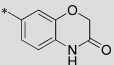
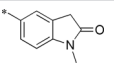
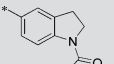
Discussion

Here, we report the discovery of VU625, the first sub-micromolar inhibitor of a mosquito Kir channel. VU625 is one of 283 confirmed *AeKir1* inhibitors identified in a HTS of approximately 30,000 compounds from the VICB library. It was chosen for lead optimization based on its potency (IC₅₀ = 96.8 nM), greater than 80-fold selectivity for the *AeKir1* channel over 8 mammalian Kir channels, and clean ancillary pharmacology among a panel of 68 critical mammalian off-targets comprised of voltage-gated ion channels, ion transporters, and receptors (i.e., neurotransmitter, peptide, and G-protein coupled). VU625 is the most potent and selective mosquito Kir channel inhibitor reported to date.

This study provides proof-of-concept that conventional drug discovery approaches can be employed successfully to identify small-molecule tools for probing the physiology of insect Kir channels and potential lead compounds for insecticide development. A similar approach has been used recently in insecticide discovery efforts targeting mosquito G-protein coupled receptors [27].

VU625 exhibits inhibitory activity against both *AeKir1* and *AeKir2B*, albeit with greater affinity for *AeKir1*. To date, we have reported the activity of two other small-molecule inhibitors of mosquito Kir channels that exhibit differential pharmacology. VU590 is a selective inhibitor of *AeKir1* over *AeKir2B*, whereas VU573 inhibits *AeKir1* and activates *AeKir2B* [6]. Thus, VU625 potentially represents a broad-spectrum, small-molecule blocker of mosquito Kir channels, pending the characterization of its effects on the other mosquito Kir channels (*AeKir2A*, *AeKir2B'* and *AeKir3* channels), which to date have not yet been expressed functionally in a heterologous system ([12]; Denton and Piermarini, personal observations). Once the distinguishing pharmacological properties of each of these Kir channel inhibitors are fully characterized, they can potentially be employed to determine the relative contributions of Kir channel subtypes in the physiology of various mosquito tissues. This would provide an important

Table 3. Structure-activity relationships and lead optimization summary for the central core portion of VU0077625 scaffold.

Cmpd	R	VU#	IC ₅₀ ±SEM (μM)
4a		VU0481807	0.55±0.08
4b		VU0486620	0.97±0.10
4c		VU0481811	>30
4d		VU0483082	>30
4e		VU0483402	>30
4f		VU0483404	1.15±0.05

IC₅₀ values were derived from 11-point CRCs on *AeKir1* in TI⁺ flux experiments performed in triplicate on two separate days.
doi:10.1371/journal.pone.0110772.t003

chemical tool set to validate and complement studies of mosquito Kir channels that employ functional genetic approaches (e.g., RNA interference).

Given the superior *in vitro* potency of VU625 compared to the *AeKir1* inhibitors VU573 [5] and VU590 [6], we expected VU625 to elicit superior *in vivo* toxicity. Thus, we were surprised when high doses of VU625 elicited no observable effects on mosquito survival or excretory capacity when injected directly into the hemolymph. Since mosquitoes have evolved robust protective mechanisms for detoxifying and excreting xenobiotics that would harm them otherwise [28,29], we investigated whether the molecule may be detoxified and/or excreted.

Preliminary experiments with PBO did not improve the efficacy of VU625, suggesting that detoxification of the compound by cytochrome P450s is unlikely to contribute to its poor *in vivo* efficacy. The co-injection of VU625 with probenecid rescued not only its toxicity, but also its effects on excretory capacity, which suggests that VU625 is likely a substrate of OATs and/or ABC transporters in the mosquitoes and may be rendered ineffective *in vivo* through excretion.

The potent toxicity of VU625 when co-injected with probenecid may be due to the ability of VU625 to inhibit at least two Kir channels, some of which are expressed in the central and peripheral nervous systems, such as Kir1 and Kir2B' [8,12,30,31], and/or a synergistic effect of probenecid that maintains high circulating concentrations of VU625 by preventing its renal excretion. Indeed, it is conceivable that the sulfonamide moiety in the structures of VU625 and probenecid causes them to be substrates for OATs and/or ABC transporters. Overall, these findings highlight efficient xenobiotic transport mechanisms in mosquitoes that render a nanomolar inhibitor of *AeKir1* (VU625) ineffective *in vivo*, even when introduced directly to the hemolymph. The tissues that contribute to the excretion of VU625 remain to be determined, but presumably involve the Malpighian tubules and/or gut [32,33].

Lastly, the medicinal chemistry efforts put forth in the present study may be a valuable first step in determining which structural moieties are important for the excretion of VU625 by xenobiotic transporters and/or its *in vivo* activity in mosquitoes. Future

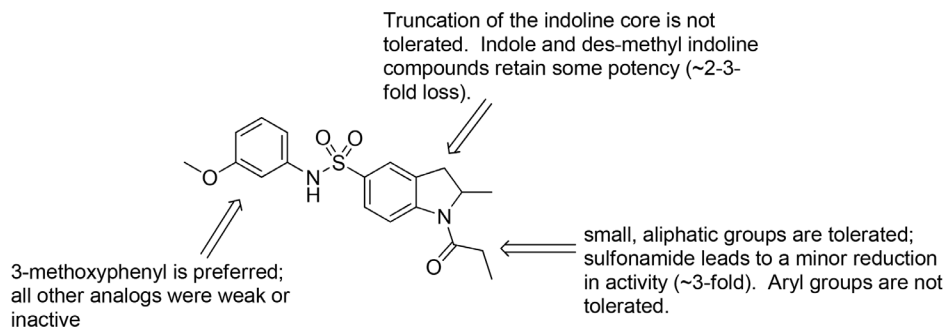


Figure 5. Summary of structure-activity relationship (SAR). Summary of observed SAR of over 100 analogs synthesized exploring all three regions of VU625.

doi:10.1371/journal.pone.0110772.g005

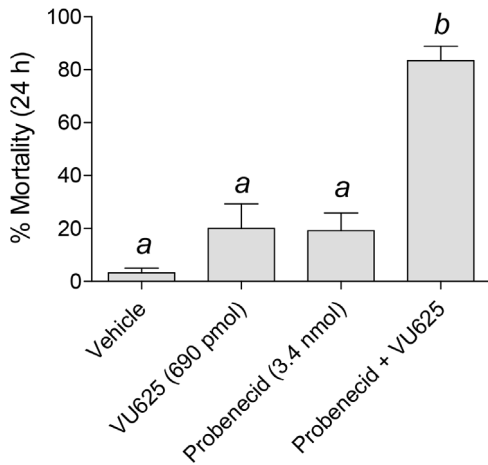


Figure 6. Effects of probenecid and VU625 on survival of adult female mosquitoes (*A. aegypti*). Percent mortality of mosquitoes at 24 h post-injection. Each mosquito was injected with 69 nl of the vehicle containing VU625 (10 mM), probenecid (50 mM), or both, to deliver the desired doses: 690 pmol of VU625, 3.4 nmol probenecid. $n=6-7$ trials of 10 mosquitoes each per treatment. Lower-case letters indicate statistical categorization of the means as determined by a one-way ANOVA with a Newman-Keuls post-test ($P<0.05$). doi:10.1371/journal.pone.0110772.g006

studies should assess the in vivo efficacy and probenecid-mediated clearance of the VU625 analog series we generated to determine if any of these compounds exhibit potent toxicity in mosquitoes without probenecid.

Perspectives

Here, we show a direct relationship between in vitro pharmacology and in vivo toxicity of VU625, which is consistent with our previous studies [5,6] suggesting that Kir channel inhibitors are promising chemicals for insecticide development. To date, none of

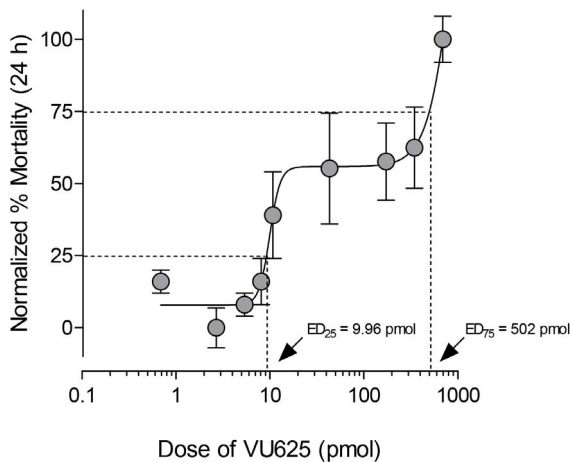


Figure 7. The dose-response curve of the toxic effects of VU625 on adult female mosquitoes (*A. aegypti*) is biphasic. Normalized percent mortality of mosquitoes at 24 h post-injection. Each mosquito was injected with 69 nL of the vehicle containing probenecid (50 mM) and an appropriate concentration of VU625 to deliver the doses of VU625 indicated and 3.4 nmol of probenecid. The ED_{25} and ED_{75} were determined by fitting a non-linear biphasic curve to the data. $n=3-4$ trials of 10 mosquitoes each per dose. doi:10.1371/journal.pone.0110772.g007

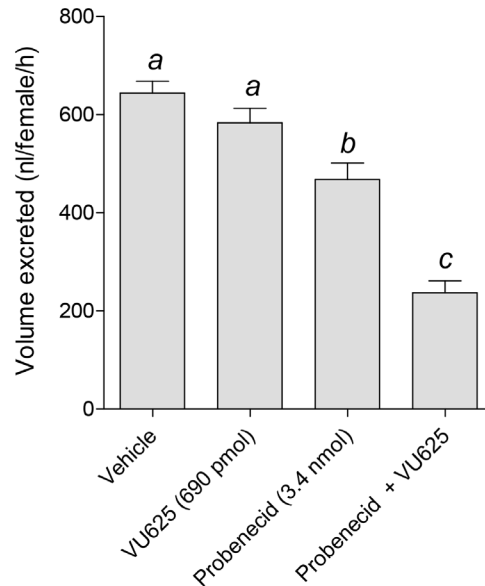


Figure 8. Effects of probenecid and VU625 on the in vivo excretory capacity of adult female mosquitoes (*A. aegypti*). Amount of urine excreted by mosquitoes 1 h after injection with 900 nL of the vehicle (K^+ -PBS₅₀ containing 1.8% DMSO, 0.077% β -cyclodextrin, and 0.008% Solutol), or the vehicle containing VU625 (0.77 mM), probenecid (3.85 mM), or both, to deliver the desired doses: 690 pmol of VU625, 3.4 nmol probenecid. Values are means \pm SEM; $n=6-18$ trials of 5 mosquitoes per treatment. Lower-case letters indicate statistical categorization of the means as determined by a one-way ANOVA with a Newman-Keuls posttest ($P<0.05$). doi:10.1371/journal.pone.0110772.g008

the Kir channel inhibitors we have reported (i.e. VU573, VU590, VU625) exhibit toxicity when applied to the cuticle (Piermarini, unpublished observations), which is a waxy, lipophilic structure that creates a physical barrier to insecticide permeation into the hemocoel of mosquitoes. This lack of topical activity severely limits the potential use of the present Kir channel inhibitors as active compounds for incorporation into insecticide-treated bed nets and indoor-residual sprays. The efficacy of common insecticides, such as permethrin, is dependent in part on their lipophilic nature [34,35]. Thus, future chemistry efforts will focus on lipophilic inhibitors of Kir channels. Furthermore, prioritizing initial HTS 'hits' according to their hydrophobicity may facilitate the discovery of more suitable small-molecules compounds for insecticide development.

Supporting Information

Figure S1 Reagents and conditions: (A) TFAA, pyridine, 0°C; (B) ClSO₃H, 40°C, 1 h; PCl₅, rt; (C) 3-methoxyaniline, DIEA, rt; MeOH:10% NaOH (1:1:1); (D) pyridine, CH₂Cl₂, ClCOCH₂CH₃. (TIF)

Figure S2 VU625 and probenecid share a sulfonamide moiety. The sulfonamide moiety contained in the chemical structure of VU625 and probenecid is shaded in blue. (TIF)

Table S1 Selectivity of VU625 against human Kir channels assessed in TI⁺ flux assays. $n=2$ independent experiments in triplicate. (DOCX)

Table S2 Summary of results obtained from the activity of the VU625 compound in radioligand binding assays.

The significant results are highlighted in grey.

(DOCX)

Table S3 SAR around the left-hand sulfonamide. IC₅₀ values were derived from 11-point CRCs on *AeKir1* in TI⁺ flux experiments performed in triplicate on two separate days.

(DOCX)

References

- WHO (2013) World Malaria Report WHO; World Health Organization.
- Ranson H, N'Guessan R, Lines J, Moiroux N, Nkuni Z, et al. (2011) Pyrethroid resistance in African anopheline mosquitoes: what are the implications for malaria control? *Trends Parasitol* 27: 91–98.
- Asidi A, N'Guessan R, Akogbeto M, Curtis C, Rowland M (2012) Loss of household protection from use of insecticide-treated nets against pyrethroid-resistant mosquitoes, benin. *Emerg Infect Dis* 18: 1101–1106.
- Maharaj R (2011) Global trends in insecticide resistance and impact on disease vector control measures. *Open Access Insect Physiology*: 27.
- Raphemot R, Rouhier MF, Hopkins CR, Gogliotti RD, Lovell KM, et al. (2013) Eliciting renal failure in mosquitoes with a small-molecule inhibitor of inward-rectifying potassium channels. *PLoS One* 8: e64905.
- Rouhier MF, Raphemot R, Denton JS, Piermarini PM (2014) Pharmacological Validation of an Inward-Rectifier Potassium (Kir) Channel as an Insecticide Target in the Yellow Fever Mosquito *Aedes aegypti*. *PLoS One* 9:e100700.
- Raphemot R, Estevez-Lao TY, Rouhier MF, Piermarini PM, Denton JS, et al. (2014) Molecular and functional characterization of *Anopheles gambiae* inward rectifier potassium (Kir1) channels: A novel role in egg production. *Insect Biochem Mol Biol* 51: 10–19.
- Döring F, Wischmeyer E, Kühnlein RP, Jäckle H, Karschin A (2002) Inwardly Rectifying K (Kir) Channels in *Drosophila*. *J Biol Chem* 277: 25554–25561.
- Evans JM, Allan AK, Davies SA, Dow JA (2005) Sulphonylurea sensitivity and enriched expression implicate inward rectifier K⁺ channels in *Drosophila melanogaster* renal function. *J Exp Biol* 208: 3771–3783.
- Eleftherianos I, Won S, Chtarbanova S, Squiban B, Ocorr K, et al. (2011) ATP-sensitive potassium channel (K_{ATP})-dependent regulation of cardiotropic viral infections. *Proc Natl Acad Sci* 108: 12024–12029.
- Dahal GR, Rawson J, Gassaway B, Kwok B, Tong Y, et al. (2012) An inwardly rectifying K⁺ channel is required for patterning. *Development* 139: 3653–3664.
- Piermarini PM, Rouhier MF, Schepel M, Kosse C, Beyenbach KW (2013) Cloning and functional characterization of inward-rectifying potassium (Kir) channels from Malpighian tubules of the mosquito *Aedes aegypti*. *Insect Biochem Mol Biol* 43: 75–90.
- Raphemot R, Kadakia RJ, Olsen ML, Banerjee S, Days E, et al. (2013) Development and validation of fluorescence-based and automated patch clamp-based functional assays for the inward rectifier potassium channel kir4.1. *Assay Drug Dev Technol* 11: 532–543.
- Hibino H, Inanobe A, Furutani K, Murakami S, Findlay I, et al. (2010) Inwardly Rectifying Potassium Channels: Their Structure, Function, and Physiological Roles. *Physiol Rev* 90: 291–366.
- Denton JS, Pao AC, Maduke M (2013) Novel diuretic targets. *Am J Physiol Renal Physiol* 305: F931–942.
- Pattnaik BR, Asuma MP, Spott R, Pillers DA (2012) Genetic defects in the hotspot of inwardly rectifying K⁺ (Kir) channels and their metabolic consequences: a review. *Mol Genet Metab* 105: 64–72.
- Denton JS, Jacobson DA (2012) Channeling dysglycemia: ion-channel variations perturbing glucose homeostasis. *Trends Endocrinol Metab* 23: 41–48.
- Lewis LM, Bhawe G, Chauder BA, Banerjee S, Lornsen KA, et al. (2009) High-throughput screening reveals a small-molecule inhibitor of the renal outer medullary potassium channel and Kir7.1. *Mol Pharmacol* 76: 1094–1103.
- Raphemot R, Lonergan DF, Nguyen TT, Utley T, Lewis LM, et al. (2011) Discovery, characterization, and structure-activity relationships of an inhibitor of inward rectifier potassium (Kir) channels with preference for Kir2.3, Kir3.x, and Kir7.1. *Front Pharmacol* 2: 75.
- Raphemot R, Swale DR, Dadi PK, Jacobson DA, Cooper P, et al. (2014) Direct Activation of beta-cell K_{ATP} Channels with a Novel Xanthine Derivative. *Mol Pharmacol*. 85: 858–65.
- Raphemot R, Weaver CD, Denton JS (2013) High-throughput screening for small-molecule modulators of inward rectifier potassium channels. *J Vis Exp*. 71: 4209.
- Niswender CM, Johnson KA, Luo Q, Ayala JE, Kim C, et al. (2008) A novel assay of Gi/o-linked G protein-coupled receptor coupling to potassium channels provides new insights into the pharmacology of the group III metabotropic glutamate receptors. *Mol Pharmacol* 73: 1213–1224.
- Bhawe G, Chauder BA, Liu W, Dawson ES, Kadakia R, et al. (2011) Development of a selective small-molecule inhibitor of Kir1.1, the renal outer medullary potassium channel. *Mol Pharmacol* 79: 42–50.
- Feller N, Broxterman HJ, Währer DC, Pinedo HM (1995) ATP-dependent efflux of calcein by the multidrug resistance protein (MRP): no inhibition by intracellular glutathione depletion. *FEBS Lett* 368: 385–388.
- Jaehde U, Sörgel F, Reiter A, Sigl G, Naber KG, et al. (1995) Effect of probenecid on the distribution and elimination of ciprofloxacin in humans. *Clin Pharmacol Ther* 58: 532–541.
- Hill G, Cihlar T, Oo C, Ho ES, Prior K, et al. (2002) The anti-influenza drug oseltamivir exhibits low potential to induce pharmacokinetic drug interactions via renal secretion-correlation of in vivo and in vitro studies. *Drug Metab Dispos* 30: 13–19.
- Meyer JM, Ejendal KF, Avramova LV, Garland-Kuntz EE, Giraldo-Calderon GI, et al. (2012) A “genome-to-lead” approach for insecticide discovery: pharmacological characterization and screening of *Aedes aegypti* D₁-like dopamine receptors. *PLoS Negl Trop Dis* 6: e1478.
- Li X, Schuler MA, Berenbaum MR (2007) Molecular mechanisms of metabolic resistance to synthetic and natural xenobiotics. *Annu Rev Entomol* 52: 231–253.
- Dermauw W, Van Leeuwen T (2014) The ABC gene family in arthropods: Comparative genomics and role in insecticide transport and resistance. *Insect Biochem Mol Biol* 45C: 89–110.
- Baker DA, Nolan T, Fischer B, Pinder A, Crisanti A, et al. (2011) A comprehensive gene expression atlas of sex- and tissue-specificity in the malaria vector, *Anopheles gambiae*. *BMC Genomics* 12: 296.
- Rouhier MF, Piermarini PM (2014) Identification of life-stage and tissue-specific splice variants of an inward rectifying potassium (Kir) channel in the yellow fever mosquito *Aedes aegypti*. *Insect Biochem Mol Biol* 48C: 91–99.
- O'Donnell MJ (2009) Too much of a good thing: how insects cope with excess ions or toxins in the diet. *J Exp Biol* 212: 363–372.
- O'Donnell MJ (2008) Insect Excretory Mechanisms. In: Simpson SJ, editor. *Advances in Insect Physiology*. London: Academic Press. pp.1–122.
- Tice CM (2001) Selecting the right compounds for screening- does Lipinski's Rule of 5 for pharmaceuticals apply to agrochemicals? *Pest Manag Sci* 57: 3–16.
- Akamatsu M (2011) Importance of physicochemical properties for the design of new pesticides. *J Agric Food Chem* 59: 2909–2917.

Acknowledgments

The authors thank Nuris Acosta (The Ohio State University), and the Vanderbilt High-Throughput Screening Center for technical assistance.

Author Contributions

Conceived and designed the experiments: RR MFR DRS ED CDW KML LCK DWE SFB CH PMP JSD. Performed the experiments: RR MFR DRS ED KML LCK DWE SFB PMP. Analyzed the data: RR MFR DRS ED CDW KML LCK DWE SFB CH PMP JSD. Contributed reagents/materials/analysis tools: CDW KML LCK DWE SFB. Wrote the paper: RR MFR DRS CDW CH PMP JSD.